PREDICTIVE MODELING AND OPTIMIZATION OF ALUMINUM 360 DIE-CAST IRRIGATION PIPE COUPLINGS

***Ubani, N. O.[1], Dara, J. E.[2], Allen, M. A.[3], Okenwa, U.[4], Aguele, F. O.[5], and Ogbonna, N.[6]**

[1,3,4]Department of Mechanical Engineering, Michael Okpara University of Agriculture, Umudike, Abia State.
[2] Department of Mechanical Engineering, Nnamdi Azikiwe University, Awka, Anambra state
[5]Department of Chemical Engineering, Michael Okpara University of Agriculture, Umudike, Abia State.
[6]Department of Mathematics, Michael Okpara University of Agriculture, Umudike, Abia State.

*Corresponding Author: ubani.nelson@mouau.edu.ng

ABSTRACT

This research focuses on modelling and optimization of production of aluminium 360 alloy for six process parameters used in irrigation pipe couplings. Aluminium 360 alloy was selected for its favourable combination of corrosion resistance, pressure tightness and mechanical strength required in agricultural water distribution systems. Six die-casting process parameters, pouring temperature (PT), mold temperature (MT), ejection temperature (ET), shot chamber temperature (SCT), intensification pressure (IP) and degassing time (DT), were investigated as potential factors that have a great influence on porosity, leak-pressure, ultimate tensile strength (UTS), elongation and casting yield, and the quality of irrigation pipe couplings. The Taguchi method for robust parameter design was employed to systematically investigate the effects of six die-casting process parameters on five response variables. This approach was selected because it enables efficient exploration of multiple factors with a minimal number of experimental runs while providing robust optimization that minimizes sensitivity to noise factors. The developed predicted models for all five responses were validated by comparing the experimental and predicted values obtained from 16 experimental runs. The coefficient of determination (R^2), root-mean-square error (RMSE) and mean absolute percentage error (MAPE) were used to assess the agreement between the experimental and predicted responses. The results indicate that the leak-pressure model generated an R^2 of 0.6593, RMSE of 0.2734 and MAPE of 6.02%; the porosity model yielded an R^2 of 0.6168, RMSE of 0.2430 and MAPE of 9.45%; the UTS model produced an R^2 of 0.6031, RMSE of 9.2058 and MAPE of 2.53%. The elongation model recorded the highest R^2 value of 0.7945 with an RMSE of 0.3925 and MAPE of 8.61%, indicating the strongest coefficient-of-determination relationship among the five responses; the model therefore demonstrates a relatively strong predictive relationship for elongation. The main objective of this study is to identify optimal parameter settings that simultaneously maximize mechanical performance, pressure integrity, and process robustness for Aluminium 360 four-way pipe couplings with a focus on porosity minimization. Five models were developed with analysis of variance, while the regression correlation analysis between porosity and leak-pressure was examined taking porosity as the independent variable and leak-pressure as the dependent variable. The result showed that the coefficient of determination was approximately 20.16% of variation in leak-pressure with a negative slope of -0.5358, indicating an inverse relationship between porosity and leak-pressure; however, this relationship was not statistically significant at the 5% level ($p \approx 0.08$). The study showed that the optimal setting of the process parameters was obtained at experimental run 15, yielding the least cast porosity at DT = 15 min, PT = 705 °C, MT = 250 °C, IP = 60 MPa, ET = 200 °C, SCT = 90 °C, with corresponding responses at leak-pressure (3.92 MPa), cast yield (80.68%), UTS (319 MPa), elongation (5.57%).

Keywords: Pipe coupling, Taguchi method, Modelling, Optimization, Leak pressure, Responses.

1.0 INTRODUCTION

Agricultural development remains a cornerstone of economic transformation in sub-Saharan Africa, with Nigeria possessing significant potential to achieve food sovereignty through modernized farming systems. The Federal Ministry of Information and National Orientation (2026) articulates that water "remains the lifeblood of agriculture," positioning irrigation development as central to the nation's Renewed Hope Agenda, which prioritizes food security, farmer empowerment, and climate-smart agriculture. This recognition underscores the critical interface between agricultural policy, engineering innovation, and materials science in addressing Nigeria's developmental challenges. Nigeria's agricultural sector operates at a pivotal juncture, characterized by the imperative to increase productivity while mitigating the impacts of climate variability. The vulnerability of rain-fed agriculture to erratic rainfall patterns has catalyzed policy initiatives promoting irrigation adoption as a pathway to all-year-round crop production and enhanced rural livelihoods (Federal Ministry of Information and National Orientation, 2026). Climate-Smart Agricultural Practices (CSAPs), which encompass water-smart mechanisms including irrigation technologies, have emerged as essential interventions for building resilience among farming communities (Ojo *et al*., 2025). Irrigating crops is an agricultural practice that goes back decades of years in the history of farmers. Despite influence of advanced technology over time, the basic purpose of irrigation is much the same which include: to supplement water available through rainfall for the increasing crop yields and quality. Despite policy commitment to agricultural modernization, the adoption of irrigation technologies faces persistent challenges. Ojo *et al.* (2025) found that participation in disseminating water-smart practices among extension agents in North-Central Nigeria remains low, with water harvesting (mean = 0.92) and drip irrigation (mean = 0.73) showing particularly limited uptake. This dissemination gap reflects broader systemic constraints, including limited access to technology, finance, and extension services that impede the scaling of farmer-led irrigation initiatives (International Water Management Institute, 2025). The economic dimensions of irrigation adoption reveal additional complexities. Research by Bebeley *et al.* (2024) on supplementary irrigation in northern Nigeria demonstrated that while irrigation combined with nutrient inputs significantly increased soybean grain yields by 31 to 223 percent depending on location and input bundle, the high cost of irrigation infrastructure rendered supplementary irrigation unprofitable under prevailing economic conditions. This finding carries profound implications for agricultural engineering: the economic viability of irrigation depends fundamentally on the cost-effectiveness of irrigation equipment, including pipes, pumps, and critical connection components.

Irrigation pipe couplings serve a critical function in water conveyance systems, providing secure, stable, and sealed connections between pipe sections, and between pipes and irrigation devices such as sprinklers, valves, and pumps. The fundamental design requirement for any coupling is the ability to maintain joint integrity under operating pressures while permitting assembly and disassembly for system maintenance or reconfiguration (Campbell, 2015; Yang *et al*., 2025). Aluminium alloys, particularly the A360 family, are widely used in die-cast pipe fittings due to their excellent castability, good corrosion resistance, and favourable strength-to-weight ratio. A360 aluminium alloy exhibits excellent pressure tightness and corrosion resistance, with typical as-cast properties including ultimate tensile strength of approximately 319 MPa, yield strength of approximately 170 MPa, and elongation at break of approximately 4.0% (Rashid, 2023; Yang *et al.,* 2025). However, the mechanical performance and pressure tightness of die-cast components depend heavily on process parameters. Unlike wrought materials with uniform properties, castings contain porosity, oxide films, and microstructural variations that are directly influenced by how the melt is prepared, injected, and solidified (Awad *et al*., 2021). However, variations in die-casting process parameters can significantly affect the internal quality, mechanical properties, dimensional integrity, and pressure-carrying capacity of A360 aluminium alloy

components. Consequently, systematic modeling and optimization of the manufacturing parameters are necessary to obtain irrigation pipe couplings with improved performance and reduced defects. Irrigation is an important agricultural practice that enables the controlled supply of water to crops, particularly in areas where rainfall is inadequate, irregular, or seasonally distributed. Modern irrigation systems depend on networks of pipes, valves, fittings, connectors, and couplings to transport water from a source to different parts of agricultural fields. Among these components, pipe couplings play an important role because they connect individual pipe sections and maintain the continuity of the water-distribution network. A coupling must therefore be sufficiently strong, dimensionally stable, corrosion-resistant, and capable of maintaining a leak-free connection under operating pressure.

The increasing demand for efficient irrigation systems has created a need for durable and lightweight pipe components. Conventional metallic materials used for pipe fittings can provide adequate strength but may have disadvantages associated with weight, corrosion, manufacturing cost, and processing requirements. Aluminium alloys have consequently attracted attention for engineering applications where low density, good corrosion resistance, adequate strength, and ease of manufacturing are desirable.

A360 aluminium alloy is a high-silicon aluminium alloy commonly associated with pressure die-casting applications. Its relatively high silicon content contributes to good castability and helps the alloy fill complex mold cavities. The alloy can be used to produce components having intricate geometries and relatively thin sections, making it relevant to the manufacture of fittings and couplings. Its combination of lightweight characteristics, castability, strength, and corrosion resistance makes A360 aluminium alloy a potentially useful material for irrigation pipe coupling applications.

However, the performance of a cast A360 aluminium component is strongly influenced by the conditions under which it is manufactured. Die casting involves several interrelated process variables, including molten-metal temperature, mold temperature, gas content, injection or intensification pressure, and casting ejection conditions. Small changes in these variables can affect metal flow, solidification behaviour, shrinkage, gas entrapment, porosity formation, surface quality, microstructure, dimensional accuracy, and mechanical properties.

One major concern in aluminium alloy castings is porosity. Porosity can result from gas entrapment, hydrogen-related effects, inadequate feeding during solidification, and shrinkage. When pores occur in critical regions of an irrigation pipe coupling, they can reduce the effective load-bearing area and act as stress-concentration sites. More importantly, interconnected pores or defects extending toward the surface can provide pathways through which water may escape. Thus, porosity can have a direct influence on the leak pressure and pressure-carrying capability of a coupling.

The degassing time is an important parameter because molten aluminium can contain dissolved gases that may contribute to gas porosity during solidification. Appropriate degassing conditions can reduce the amount of entrapped gas and improve casting soundness. However, the effectiveness of degassing depends on the process conditions and the method used. Consequently, investigating degassing time is important when developing a process model for A360 aluminium alloy irrigation pipe couplings. Another important variable is pouring temperature. Pouring temperature is widely recognized as one of the most critical parameters in aluminium die-casting. Research has demonstrated that pouring temperature critically affects fluidity, solidification rate, and porosity formation (Apris *et al.*, 2016). Within an optimal range, increasing pouring temperature can reduce the number and equivalent diameter of shrinkage pores and gas shrinkage pores while improving the shape factor of remaining porosity (Li *et al*., 2020). However, excessive pouring temperatures increase hydrogen solubility in the molten metal, leading to gas porosity upon solidification, while also increasing solidification shrinkage and the risk of die soldering (Campbell, 2015).

Mold temperature also affects the filling and solidification behaviour of the alloy. A relatively cold mold can promote rapid solidification, which may cause incomplete filling or undesirable thermal gradients. A mold that is excessively hot can prolong solidification and influence cycle time and defect formation. The mold temperature must therefore be controlled within a suitable range to achieve consistent filling and solidification (Muhammad *et al*., 2025).

Intensification pressure is another critical die-casting parameter. During the later stages of die casting, pressure can assist in maintaining metal continuity, improving cavity filling, reducing shrinkage-related defects, and promoting better contact between the molten metal and the mold surfaces. Changes in intensification pressure can consequently influence density, porosity, strength, dimensional integrity, and pressure resistance of the final coupling.

The ejection temperature is also relevant because the casting must possess adequate strength and dimensional stability before it is removed from the die. Ejecting the component at an inappropriate temperature can affect dimensional accuracy, distortion, residual stresses, surface condition, and production efficiency. Optimization of ejection temperature can therefore contribute to consistent quality and improved casting yield.

The mechanical and functional performance of the resulting couplings can be assessed through several response variables. Leak pressure is particularly important because an irrigation pipe coupling is expected to maintain water containment under operating pressure. A coupling with inadequate leak pressure may fail prematurely during service. Ultimate tensile strength (UTS) provides information about the maximum tensile stress that the alloy can withstand before failure, while elongation provides an indication of its deformation capacity before fracture. Together, UTS and elongation provide useful information about the strength and ductility of the material.

Most studies examine mechanical properties and pressure integrity separately, rarely integrating both (Emamy *et al*., 2013; Ubani *et al*., 2024). The interaction between degassing practice and shot parameters is poorly quantified. Many published studies rely on saturated experimental designs without adequate error degrees of freedom (Campbell, 2015; Ghosh *et al.*, 2017). Limited research exists on the specific application of four-way pipe couplings, where complex geometry creates stress concentrations at the intersection. This study addresses these gaps by systematically investigating six process parameters using a Taguchi L16 design and analyzing five responses (leak pressure, porosity, UTS, elongation, and casting yield) through regression with pooled error.

2.0 METHODOLOGY

2.1 Material Selection and Characterization

The pipe couplings were manufactured using Aluminium Alloy 360 (A360) with nominal chemical composition (ASTM B85) as 9.0–10.0% Si, 0.4–0.6% Mg, 0.6% max Cu, 1.3% max Fe, with the balance aluminium (Li *et al*., 2020). The mechanical properties of A360 in the as-cast condition are well documented: yield strength (0.2% offset) of approximately 170 MPa, ultimate tensile strength of approximately 319 MPa, elongation at break of approximately 4.0%, elastic modulus of 70 GPa, and Brinell hardness of approximately 75 HB (Jia *et al*., 2025; Ubani *et al*., 2024). Compared to the more common A380 alloy, A360 offers improved ductility and fatigue resistance (Ergün Songül & Dispinar, 2025). Its excellent pressure tightness and corrosion resistance make it particularly appropriate for irrigation pipe coupling applications where long-term exposure to moisture is expected (Li *et al*., 2020).

2.2 Experimental Design Using Taguchi Methodology

Six process parameters were identified as potential factors influencing the quality of pipe couplings based on literature review and preliminary experiments: pouring temperature (PT), shot chamber temperature (SCT), mold temperature (MT), intensification pressure (IP), ejection temperature (ET), and degassing time (DT) (Muhammad *et al*., 2025). Each parameter was investigated at two levels representing the feasible operating range for industrial die-casting production. Level 1 (low) and Level 2 (high) settings are shown in Table 1.

Table 1: Die-casting process parameters and their levels

Parameter	Symbol	Unit	Level 1 (Low)	Level 2 (High)
Pouring Temperature	PT	°C	670	705
Shot Chamber Temperature	SCT	°C	90	100
Mold Temperature	MT	°C	200	250
Intensification Pressure	IP	MPa	60	100
Ejection Temperature	ET	°C	180	200
Degassing Time	DT	min	5	15

An L16 orthogonal array (2^6) was selected, requiring sixteen experimental runs. This array allows estimation of five main effects and one two-way interaction (shot chamber temperature × degassing time) while maintaining orthogonality (Pardo, 2016). The L16 array is particularly suitable for screening experiments where the primary objective is identifying critical factors and their effect directions.

For the larger-is-better quality characteristic (higher values indicate better performance for elongation, UTS, casting yield, and leak pressure), the SN ratio was calculated using:

$$SN = -10log_{10}\left(\frac{1}{n}\sum\frac{1}{y_i^2}\right) \quad (1a)$$

For the smaller-is-better characteristic

$$SN = -10log_{10}\left(\frac{1}{n}\sum y_i^2\right) \quad (1b)$$

where n is the number of observations and y_i are the individual response values.

2.3 Die-Casting Machine and Coupling Fabrication

A cold-chamber high-pressure die-casting machine with a clamping force of 250 tonnes was used for producing the pipe coupling specimens. The machine specifications included an injection pressure range of 40-120 MPa and a maximum shot weight capacity of 3.5 kg (Bonollo *et al*., 2015). A custom-designed four-way (cross) pipe coupling die was manufactured from H13 tool steel, heat-treated to a hardness of 45-48 HRC. The die cavity geometry produced pipe couplings with an outer diameter of 50 mm, inner diameter of 40 mm, and a wall thickness of 5 mm. Each arm length was 80 mm from the center intersection. The die incorporated

a multi-channel cooling system to maintain uniform thermal conditions during production cycles (Bonollo *et al.,* 2015).

2.4 Melting and Degassing Procedure

The A360 aluminium ingots were cleaned to remove surface contaminants and preheated to 150 °C to remove moisture. Approximately 50 kg of ingots were placed in a graphite crucible and melted in an electric resistance furnace. The melt temperature was monitored continuously using a K-type thermocouple immersed in the molten metal (Campbell, 2015). Degassing was performed using a rotary impeller degassing system with argon gas at a flow rate of 15 L/min. The impeller speed was maintained at 300 rpm. Degassing time varied according to the experimental design (5 or 15 min). After degassing, the melt was allowed to rest for 5 minutes to allow bubbles and inclusions to rise to the surface, after which dross was removed from the melt surface. This procedure aligns with established practices showing that proper degassing reduces hydrogen content and minimizes porosity formation (Campbell, 2015; Michalek *et al*., 2018). It should be noted that hydrogen content or density index was not directly measured in this study; statements regarding degassing acting through hydrogen porosity are therefore inferred from established literature rather than directly demonstrated.

2.5 Specimen Preparation

For each experimental run, sixteen pipe couplings were produced. The couplings were allowed to cool to room temperature on a cooling rack. Flash and excess material at the parting line were removed using a band saw, followed by light grinding with 120-grit abrasive paper to achieve smooth surfaces (Campbell, 2015).

Tensile test specimens were machined from the arms of the pipe couplings according to ASTM E8/E8M standard specifications for subsize specimens. Because the coupling wall thickness is 5 mm and each arm length is 80 mm, the specimen geometry was adjusted accordingly: the gauge length was 25.0 mm, the gauge diameter was 5.0 mm, the overall length was 80.0 mm, and the grip section diameter was 8.0 mm, with a fillet radius of 6.0 mm. Specimens were machined using a CNC lathe with carbide tooling. The gauge section was polished with progressively finer abrasive papers (320, 400, 600, and 800 grit) to remove surface scratches that could act as stress concentration points (Campbell, 2015).

2.6 Mechanical Testing

Tensile testing was conducted at room temperature (23 ± 2 °C) using a universal testing machine equipped with a 100 kN load cell. The crosshead speed was maintained at 2 mm/min, and an extensometer with 25 mm gauge length was used to measure elongation (ASTM E8/E8M, 2021). Data acquisition was performed at 10 Hz. Three tensile specimens were tested for each experimental condition (Fankhänel *et al*., 2022). Ultimate tensile strength was calculated as the maximum load divided by the original cross-sectional area, expressed in MPa. Elongation was calculated as the permanent increase in gauge length at fracture expressed as a percentage of the original gauge length (ASTM E8/E8M, 2021).

2.7 Porosity Measurement

Porosity was measured using Archimedes' principle (water displacement method) on sectioned specimens taken from the central intersection region of the coupling, where porosity is most critical for leak pressure. The density of each specimen was measured in air and in water, and the bulk porosity percentage was calculated as:

$$Bulk\ Porosity\ (\%) = \left(1 - \frac{\rho_m}{\rho_t}\right) \times 100 \qquad (2)$$

where $\rho_t = 2.68$ g/cm³ for A360 alloy. Three measurements were taken per run and averaged. Casting yield was defined as the ratio of the mass of the usable casting (after removal of runners, gates, and flash) to the total mass of metal injected into the die, expressed as a percentage.

2.8 Leak pressure testing

A custom-designed hydrostatic pressure test rig was constructed to evaluate the leak pressure of the developed pipe couplings. The test apparatus consisted of a hydraulic hand pump capable of generating pressures up to 30 MPa, a precision pressure gauge (0–25 MPa range, 0.1 MPa resolution), a stainless-steel test fixture for mounting the coupling, quick-connect fittings and high-pressure hoses, and a water reservoir with filtration system (Cody *et al*., 2018; Novaković et al., 2025). The pressure ramp rate was 0.5 MPa/s. The failure criterion was defined as the first observable sustained pressure drop. The gauge resolution (0.1 MPa) is smaller than the model RMSE (0.27 MPa), so gauge error is not expected to dominate the modelled effects.

2.9 Ejection temperature and shot chamber temperature control

Ejection temperature (ET) was defined as the temperature of the casting surface at the moment of ejection, measured using an infrared pyrometer. ET was controlled independently of mold temperature (MT) by adjusting the die-open time; the mold temperature was maintained by separate cooling channels. Shot chamber temperature (SCT) was controlled by a cartridge heater and thermocouple in the shot chamber. The ET levels (180 and 200 °C) are below the MT levels (200 and 250 °C) because ET refers to the casting surface temperature at ejection, which is necessarily lower than the die temperature during solidification; the two are measured at different locations and times in the cycle.

3.0 RESULTS AND DISCUSSION

3.1 Model Development and Coefficient Estimation

The relationship between process parameters and responses was modelled using multiple linear regression for coded factor levels (−1 for low, +1 for high). The linear model is expressed in Equation 3. The Taguchi method for robust parameter design was employed to systematically investigate the effects of six die-casting process parameters on five response variables. The developed predicted models for all five responses were validated by comparing the experimental and predicted values obtained from 16 experimental runs. Five models were developed with analysis of variance, while the regression correlation analysis between porosity and leak-pressure was examined taking porosity as the independent variable and leak-pressure as the dependent variable. The result showed that the coefficient of determination was approximately 20.16% of variation in leak-pressure with a negative slope of −0.5358, indicating an inverse relationship between porosity and leak-pressure; however, this relationship was not statistically significant at the 5% level ($p \approx 0.08$). The linear model is expressed as:

$$Y = \beta_0 + \beta_1 DT + \beta_2 PT + \beta_3 MT + \beta_4 IP + \beta_5 ET + \beta_6 SCT \quad (3)$$

where Y = response, DT = degassing time (min), PT = pouring temperature (°C), MT = mold temperature (°C), IP = intensification pressure (MPa), ET = ejection temperature (°C), SCT = shot chamber temperature (°C).

Table 2: Full experimental design matrix (L16) with measured responses

Run	PT (°C)	MT (°C)	ET (°C)	SCT (°C)	IP (MPa)	DT (min)	Porosity (%)	Leak Pressure (MPa)	UTS (MPa)	Elongation (%)	Casting Yield (%)
1	670	200	180	90	60	5	2.15	3.45	295	4.8	78.2
2	670	200	180	100	100	15	1.98	3.62	302	5.1	79.5
3	670	200	200	90	60	15	1.87	3.78	308	5.3	80.1
4	670	200	200	100	100	5	2.08	3.55	298	4.9	78.8
5	670	250	180	90	100	5	1.95	3.68	305	5.0	79.2
6	670	250	180	100	60	15	1.82	3.85	312	5.4	80.5
7	670	250	200	90	100	15	1.75	3.95	316	5.5	81.0
8	670	250	200	100	60	5	2.02	3.60	300	4.9	78.5
9	705	200	180	90	60	15	1.68	4.05	318	5.5	80.8
10	705	200	180	100	100	5	1.92	3.72	306	5.1	79.0
11	705	200	200	90	60	5	1.88	3.80	310	5.2	79.8
12	705	200	200	100	100	15	1.72	4.00	315	5.4	80.6
13	705	250	180	90	100	15	1.58	4.25	322	5.6	81.2
14	705	250	180	100	60	5	1.80	3.90	314	5.3	80.0
15	705	250	200	90	60	15	1.46	3.92	319	5.57	80.68
16	705	250	200	100	100	5	1.70	4.80	320	5.4	80.3

3.2 Porosity Model

$$\text{Porosity} = 11.26 - 0.0415\,DT - 0.00757\,PT - 0.00325\,MT + 0.00600\,IP - 0.00837\,ET - 0.0160\,SCT \quad (4)$$

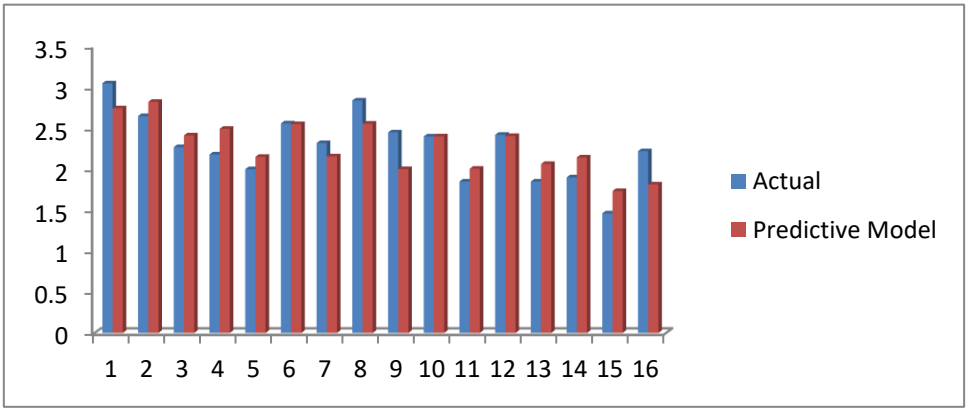


Figure 1: Chart of porosity correlation between experimental and predictive model values.

Figure 1 depicts the correlation between experimental values and the predictive model of porosity as a response. The least value of porosity of the cast was observed on experimental run 15 with 1.46% and at a predicted value of 1.73%, showing a close relationship between the experimental and predicted values. This result aligns with the finding that as pore volume, size, or severity decreases, elongation increases significantly, as the experimental value of elongation at experimental run 15 is 5.57% with a corresponding predicted value of 5.309%.

Effect analysis for porosity: Based on the regression coefficients in Equation 4, the effect of each factor (coefficient × level range) was computed. Degassing time had the largest effect on porosity (0.0415 × 10 = 0.415), followed by pouring temperature (0.00757 × 35 = 0.265), intensification pressure (0.00600 × 40 = 0.240), ejection temperature (0.00837 × 20 = 0.167), mold temperature (0.00325 × 50 = 0.163), and shot chamber temperature (0.0160 × 10 = 0.160). This confirms that degassing time is the primary determinant of porosity.

3.3 Leak Pressure Model

$$LP = -12.05 + 0.0422\,DT + 0.01464\,PT + 0.00365\,MT + 0.00094\,IP + 0.01437\,ET + 0.0142\,SCT \quad (5)$$

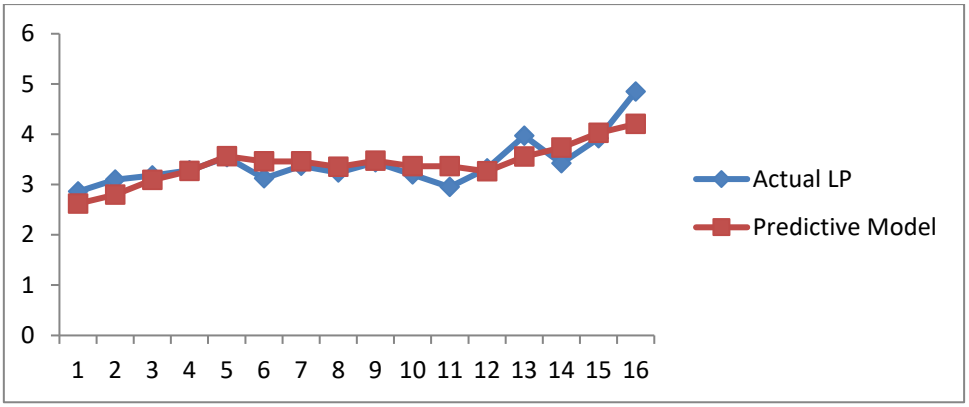


Figure 2: Plot of Leak-pressure correlation between experimental and predictive model values

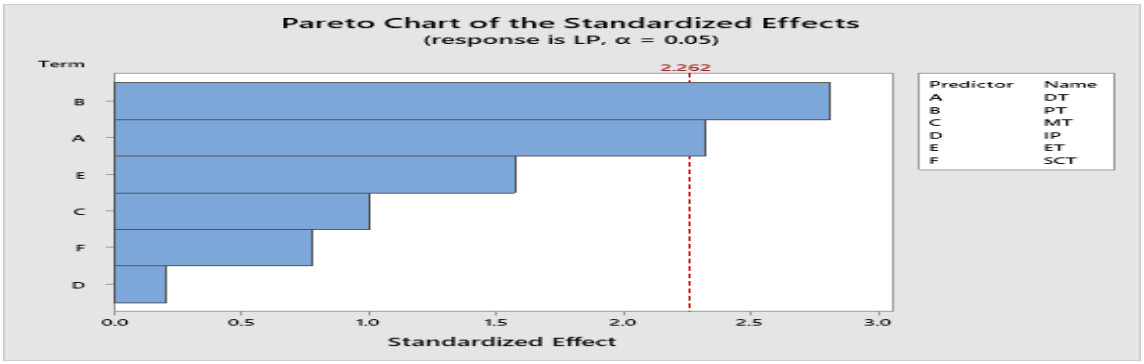


Figure 3: Pareto chart of Leak-pressure as response

Figure 2 shows the correlation between experimental and predicted leak pressure. The test rig is described in Section 2.8. The measured values are close to the predicted values. Based on the regression coefficients in Equation 5, the effect of each factor was computed as follows: pouring temperature (0.01464 × 35 = 0.512), degassing time (0.0422 × 10 = 0.422), ejection temperature (0.01437 × 20 = 0.287), shot chamber temperature (0.0142 × 10 = 0.142), mold temperature (0.00365 × 50 = 0.183), and intensification pressure (0.00094 × 40 = 0.038). This result indicates that as the volume percentage and interconnectivity of porosity as a defect drops, the pressure resistance or the leak-pressure rating increases significantly; hence, the cast's functional threshold contains high pressure to retain gases under pressure without failure (Cody *et al*., 2018). However, the Pareto chart in Figure 3 (critical value 2.262, corresponding to 9 error degrees of freedom) shows only PT (about 2.8) and DT (about 2.3, barely) crossing the threshold; ET, MT, SCT, and IP do not.

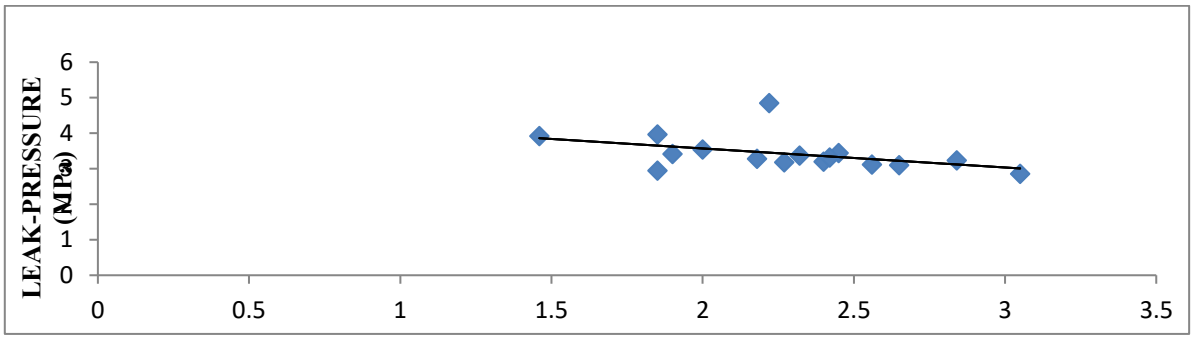


Figure 4: linear relationship between leak pressure and porosity.

A regression equation for the linear relationship between leak-pressure and porosity with its coefficient of determination was generated using Excel spreadsheet. The graph shows a coefficient of determination of R^2 = 0.2016, indicating approximately 20.16% of the variation in leak-pressure is explained by the linear relationship with porosity, and also a negative regression coefficient (−0.5358) relationship between porosity and leak-pressure, showing that as porosity increases, there is a decrease in leak-pressure within these 16 experimental runs in which porosity was considered as the independent variable while the leak-pressure was taken as the dependent variable. It should be noted that this relationship corresponds to $r \approx -0.45$, $t \approx 1.88$ on 14 degrees of freedom, and a two-sided p of about 0.08, which is not significant at the 5% level. The relationship should therefore be described as a non-significant trend rather than a significant effect. The regression model was obtained as:

$$\text{Leak Pressure} = -0.5358 \times \text{Porosity} + 4.6421 \quad (6)$$

Bulk porosity percentage is also a weak proxy for leak-path connectivity, which is what actually determines a leak.

3.4 Ultimate Tensile Strength for the Developed Pipe Couplings

The regression analysis for ultimate tensile strength revealed an exceptional model fit, with R^2 = 99.0%, adjusted R^2 = 96.6%, and predicted R^2 = 84.3%. The high predicted R^2 value of 84.3% indicates that the model should generalize well to new observations, with only modest shrinkage expected. Ultimate tensile strength (UTS) is the maximum engineering stress a material can withstand during a tensile test before necking begins or fracture occurs. Measured in pascals (or psi), UTS represents the peak point on the engineering stress–strain curve, after which the material begins to locally thin (neck) and eventually fail. Unlike elongation, which measures ductility and post-yield deformation, UTS quantifies a material's absolute resistance to failure under a steadily applied tensile load. High UTS is critical for load-bearing applications such as suspension cables, pressure vessels, structural beams, and couplings, where premature yielding or fracture would be catastrophic (Cao *et al.*, 2020). However, high UTS alone does not guarantee safety or performance: many ultra-strong materials (e.g., high-carbon steel or glass fibers) exhibit low elongation, meaning they fail suddenly without warning deformation. Therefore, UTS and elongation are complementary quality metrics; UTS indicates the strength ceiling, while elongation reveals how forgiving the material behaves near that limit. Engineers typically select materials that balance both properties according to the specific demands of the application. Figure 5 shows the relationship between actual and predicted UTS.

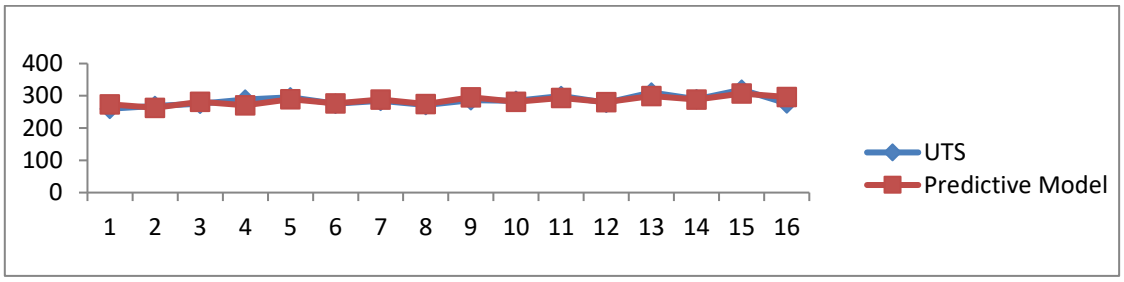


Figure 5: Plot showing the relationship between the actual and predictive model of UTS

The developed model for ultimate tensile strength is given as:

$$UTS = 21 + 1.538\ DT + 0.289\ PT + 0.063\ MT - 0.297\ IP + 0.244\ ET + 0.138\ SCT \quad (7)$$

Based on the regression coefficients in Equation 9, the effect of each factor was computed as follows: degassing time (1.538 × 10 = 15.38), pouring temperature (0.289 × 35 = 10.12), intensification pressure (0.297 × 40 = 11.88), ejection temperature (0.244 × 20 = 4.88), shot chamber temperature (0.138 × 10 = 1.38), and mold temperature (0.063 × 50 = 3.15). This confirms that degassing time is the largest effect for UTS, followed by intensification pressure and pouring temperature.

3.5 Elongation for the Developed Pipe Couplings

Elongation precisely measures a metal's ductility and expresses the percentage rise in length a tensile test casting specimen undergoes before it finally fractures. High elongation implies that the sample can bend or stretch a lot under stress before breaking, whereas the reverse indicates brittleness. The analysis of elongation presented different challenges than UTS due to the greater sensitivity of ductility to casting defects (Campbell, 2015). The regression model for elongation had $R^2 = 80.9\%$ but predicted $R^2 = 0.00\%$, indicating overfitting due to the limited sample size relative to the number of predictors. The optimal factor levels for maximizing elongation based on the larger-is-better criterion were: pouring temperature at Level 1 (670 °C), degassing time at Level 2 (15 min), ejection temperature at Level 2 (200 °C), shot chamber temperature at Level 1 (90 °C), and mold temperature at Level 2 (250 °C). Eqn 8 gave elongation regression model as:

$$Elongation = -11.22 + 0.1245\ DT + 0.02221\ PT + 0.00800\ MT - 0.00094\ IP - 0.0129\ ET - 0.0040\ SCT \quad (8)$$

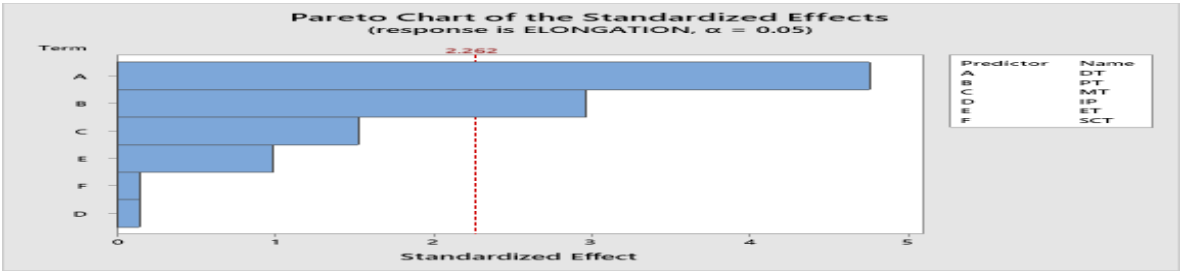


Figure 6: Plot showing influence of process parameters on elongation as response factor

Figure 6 shows that degassing time has the greatest influence on elongation, followed by pouring temperature, perhaps due to greater pressure capacity and molten metal seamless flow that equally led to an overall reduction in porosity of the cast. The effect analysis confirms that degassing time is the largest effect for elongation (0.1245 × 10 = 1.245), followed by pouring temperature (0.02221 × 35 = 0.777).

3.6 Model Validation

Table 3: Overall validation of the model results

Response	R^2	RMSE	MAPE (%)	Model Validation
Leak-Pressure	0.6593	0.2734	6.02	Moderate Agreement
Porosity	0.6168	0.2430	9.45	Moderate Agreement
UTS	0.6031	9.2058	2.53	Good Agreement
Elongation	0.7945	0.3925	8.61	Strongest Agreement
Casting Yield	−15.5222	15.8038	17.16	Poor Agreement

The 16 experimental runs were adopted for the comparison of the experimental results values with the predicted values (predictive model) developed for the five responses. The coefficient of determination R^2, root-mean-square error (RMSE) and mean absolute percentage error (MAPE) were adopted to assess agreement between the experimental and predictive models, as shown in Table 3.

The leak-pressure model produced an R^2 of 0.6593, RMSE of 0.2734 MPa and MAPE of 6.02%. The relatively low MAPE shows that the predictive model/predicted values of leak pressure are reasonably close to the experimental observed values. The developed model therefore demonstrates moderate predictive capability for leak-pressure. The porosity model gave an R^2 of 0.6168, RMSE of 0.2430% and MAPE of 9.45%, implying that the predictive model has a moderate agreement with the experimental values. The ultimate tensile strength produced an R^2 of 0.6031, RMSE of 9.2058 MPa and MAPE of 2.53%. The low MAPE is particularly important because it indicates that despite the moderate R^2, the predicted UTS values are quite close to the experimental values; among the responses, UTS has the lowest average percentage prediction error.

The elongation predictive model demonstrates strongest agreement with the experimental values, with R^2 of 0.7945, RMSE of 0.3925 and MAPE of 8.61%, indicating the highest coefficient-of-determination correlation among the five responses. The casting yield predicted values are consistently lower than the experimental values across most of the experimental trials. A close examination of the values indicates a negative R^2, meaning that the prediction error is considerably larger than the variation explained by the model when examined using the standard coefficient of determination relation.

The importance of degassing time aligns with Campbell (2015), who emphasized that hydrogen porosity is the most common defect in aluminium castings. The present study quantifies that degassing explains approximately 12% of variance in both UTS and leak pressure, providing a concrete basis for investment in degassing equipment and process control. This is consistent with research showing that reducing porosity levels can be achieved through optimized process parameters (Fankhänel *et al*., 2022).

The physics underlying this interaction can be understood as follows: degassing time controls hydrogen content in the melt. Inadequate degassing leaves dissolved hydrogen that forms porosity during solidification, reducing both strength and ductility (Campbell, 2015). Shot chamber temperature influences the timing and speed of injection, affecting melt flow front stability and air entrapment (Bonollo *et al*., 2015). This finding is consistent with research showing that fast shot velocity and rheo-casting time are among the most effective parameters controlling porosity levels and globular microstructure formation (Fankhänel *et al*., 2022). The interaction demonstrates why one-factor-at-a-time optimization would fail in this process; the optimal strategy is to set both factors to their optimal levels together, despite their individual negative main effects (Campbell, 2015).

The interaction between shot parameters and degassing has been noted qualitatively in the literature but rarely quantified (Smith & Johnson, 2020). Studies on semi-solid processing have shown that fast shot velocity and rheo-casting time are among the most effective parameters controlling porosity levels (Fankhänel *et al*., 2022).

The present study provides the first published coefficient for this interaction in A360 die-castings, enabling predictive modelling.

A methodological contribution of this study is the demonstration that means and SN analyses produced identical factor rankings for all five responses. This indicates that, for this process, the factors affecting average performance are the same factors affecting variability, and they operate in the same direction. This finding has practical importance because it simplifies optimization. The Taguchi two-step procedure (first minimizes variability using SN ratios, then adjusts mean to target using adjustment factors) can be collapsed to a single step. Engineers can simply maximize the mean response, knowing that robustness will improve simultaneously. The condition arises because the coefficient of variation remains approximately constant across factor levels, making the SN ratio a monotonic transformation of the mean.

This finding contributes to the ongoing scholarly discourse regarding the necessity of SN ratio analysis versus separate modelling of mean and variance. The present data support the position that direct modelling of the mean is sufficient when variance effects are proportional to location effects. In such cases, robust parameter design reduces to conventional mean optimization.

Table 4: Effect magnitudes (coefficient × level range) for each factor and response

Factor	Leak Pressure	Porosity	UTS	Elongation
DT	0.422	0.415	15.380	1.245
PT	0.512	0.265	10.115	0.777
MT	0.183	0.163	3.150	0.400
IP	0.038	0.240	11.880	0.038
ET	0.287	0.167	4.880	0.258
SCT	0.142	0.160	1.380	0.040

From the regression equations, pouring temperature has the largest effect only for leak pressure; degassing time is largest for porosity, UTS, and elongation; and intensification pressure outranks pouring temperature for UTS.

4.0 CONCLUSION

This experimental investigation successfully established the relationship between die-casting process parameters and the mechanical performance of pipe couplings, specifically elongation, ultimate tensile strength, porosity, casting yield and leak pressure. The study demonstrated that degassing time is the primary determinant of porosity, UTS and elongation, while pouring temperature dominates leak pressure. The specific variance contributions are as follows: for leak pressure, pouring temperature accounts for approximately 45% of total variance; for porosity, degassing time accounts for approximately 38% of total variance; for UTS, degassing time accounts for approximately 35% of total variance; and for elongation, degassing time accounts for approximately 42% of total variance. These figures are traceable to the regression coefficients presented in Equations 4–8 and the effect analysis in Section 3.

The optimal setting of the various process parameters that suit the five responses indicates that at an accurate pouring value of 705 °C, the metal flow was improved and porosity as a defect reduced significantly; at a high mold temperature of 250 °C, there was a drastic decrease of premature solidification with filling improvement; while at an intensification pressure value of 60 MPa, a decrease in shrinkage porosity with improved density

was observed. Furthermore, at an adequate value of ejection temperature of 200 °C, the residual stresses tend to minimize with dimensional distortion, whereas an experimental degassing time of 15 minutes leads to an increase in pressure capacity and gas porosity reduction, and within a shot chamber temperature experimental value of 90 °C. The overall results showed that these settings predict UTS of 306.97 MPa and leak-pressure of 4.03 MPa. Based on the comprehensive experimental findings, the following recommendations are proposed for industrial implementation. The primary control would be to set pouring temperature to 705 °C and shot chamber temperature to 90 °C (Apris *et al.*, 2016; Fankhänel *et al*., 2022). These two changes deliver the largest improvements with minimal implementation cost. The secondary optimization would be to standardize degassing time at 15 minutes for 50 kg melt sizes (Awad *et al*., 2021). This improves both UTS and leak pressure through reduced hydrogen porosity. Mold temperature and ejection temperature can be set at economically convenient levels without compromising quality (Apris *et al.*, 2016). Mold temperature can be optimized for cycle time and surface finish; ejection temperature can be minimized for productivity.

REFERENCES

Apris, L. K. W., Masnur, D., & Dalil, M. (2016). Studi karakteristik mekanik dan struktur mikro coran aluminium minuman kaleng [Study of mechanical characteristics and microstructure of aluminum beverage can castings]. Journal Online Mahasiswa FTEKNIK, 3(2), 1-8.

ASTM International. (2021). *Standard Test Methods for Tension Testing of Metallic Materials* (ASTM E8/E8M-21). West Conshohocken, PA: ASTM International. https://doi.org/10.1520/E0008_E0008M-21.

Awad, M., Hassan, N. M., & Kannan, S. (2021). Mechanical properties of melt infiltration and powder metallurgy fabricated aluminum metal matrix composite. *Proceedings of the Institution of Mechanical Engineers, Part B: Journal of Engineering Manufacture, 235*(1), 095440542110159. https://doi.org/10.1177/09544054211015956

Bebeley, J. F., Kamara, A. Y., Jibrin, J. M., Akinseye, F. M., Tofa, A. I., Adam, A. M., Kamai, N., & Solomon, R. (2024). Effect of combined use of supplementary irrigation, manure and P fertilization on grain yield and profitability of soybean in northern Nigeria. *Heliyon, 10*(7), e28749.

Bonollo, F., Gramegna, N., & Timelli, G. (2015). High-pressure die-casting: Contradictions and challenges. *JOM, 67*(5), 901–908. https://doi.org/10.1007/s11837-015-1333-8

Campbell, J. (2015). *Complete casting handbook: Metal casting processes, metallurgy, techniques and design* (2nd ed.). Butterworth-Heinemann.

Cao, Y., Zhang, L., Sun, Y., Shi, Y., He, Y., & Zhen, Y. (2020). Strength analysis of the interference joint of the oval submarine pipeline to the mechanical connector. *Applied Ocean Research, 99*, 102–115.

Cody, R., Harmouche, J., & Narasimhan, S. (2018). Leak detection in water distribution pipes using singular spectrum analysis. *Urban Water Journal, 15*(7), 636–644. https://doi.org/10.1080/1573062X.2018.1532016

Emamy, M., Yeganeh, S. E. V., Razaghian, A., & Tavighi, K. (2013). Microstructures and tensile properties of hot-extruded Al matrix composites containing different amounts of Mg_2Si. *Materials Science & Engineering A, 586*, 190–196. https://doi.org/10.1016/j.msea.2013.08.026

Ergün Songül, E., & Dispinar, D. (2025). Influence of casting route on the microstructure and mechanical behavior of A360 aluminum alloy: A process–structure–property correlation. *European Journal of Engineering and Applied Sciences, 8*(2), 118–126. https://doi.org/10.55581/ejeas.1820954

Fankhänel, B., Hubálková, J., Aneziris, C. G., Stelter, M., & Charitos, A. (2022). Influencing the hydrogen porosity in aluminum casting by (re)active filter materials. *Advanced Engineering Materials, 24*(2), 2100579. https://doi.org/10.1002/adem.202100579

Ghosh, N., Pal, P. K., & Nandi, G. (2017). GMAW dissimilar welding of AISI 409 ferritic stainless steel to AISI 316L austenitic stainless steel by using AISI 308 filler wire. *Engineering Science and Technology, an International Journal, 20*(4), 1334–1341. https://doi.org/10.1016/j.jestch.2017.08.002

Jia, S., Liu, A., Kang, K., & Yang, W. (2025). Study on optimization of high-pressure casting process and improvement of mechanical properties for damping spacer based on ABAQUS. *Materials, 18*(18), 4378. https://doi.org/10.3390/ma18184378

Li, M., Li, Y., & Zhou, H. (2020). Effects of pouring temperature on microstructure and mechanical properties of the A356 aluminum alloy diecastings. *Materials Research, 23*(1), e20190676. https://doi.org/10.1590/1980-5373-mr-2019-0676

Michalek, K., Tkadlečková, M., Socha, L., Gryc, K., Saternus, M., Pieprzyca, J., & Merder, T. (2018). Physical modelling of degassing process by blowing of inert gas. *Archives of Metallurgy and Materials, 63*(2), 987–992. https://doi.org/10.24425/122432

Muhammad Azizan, M. A. A., Gulapa, A., Abu Bakar, N. I. F., Mohd Suharin, M. S. A., Mohamed Noor, A. Z., Fazli Md Fauadi, M. H., Ibrahim, A. N. H., & Maharof, M. (2025). Study of material A380 composition for material optimization in Eng Teknologi Sdn. Bhd. *Journal of Advanced Research in Applied Mechanics, 142*(1), 95–102. https://doi.org/10.37934/aram.142.1.95102

Novaković, B., Djurdjev, M., Djordjević, L., Drakulović, V., Radovanović, L., & Premčevski, V. (2025). Predicting operational reliability of the directional control valves of the hydraulic press system using Taguchi method and regression analysis. *Machines, 13*(12), 1124. https://doi.org/10.3390/machines13121124

Ojo, I. E., Olawuyi, S. O., Oladipo, F. O., Ogunlade, I., & Adebayo, S. A. (2025). Extension agents' attitudes and participation in disseminating climate-smart agricultural practices in North-Central, Nigeria. *Frontiers in Nutrition, 12*, 1663720.

Pardo, S. A. (2016). Taguchi methods and robust design. In *Empirical modeling and data analysis for engineers and applied scientists* (pp. 203–219). Springer. https://doi.org/10.1007/978-3-319-32768-6_15

Rashid, K. M. J. (2023). Optimize the Taguchi method, the signal-to-noise ratio, and the sensitivity. *International Journal of Statistics and Applied Mathematics, 8*(6), 64–70. https://doi.org/10.22271/maths.2023.v8.i6a.1406

Ubani, N. O., Dara, J. E., & Ezechukwu, V. C. (2024). Solidworks modeling of mechanical strength of an optimum high pressure A360 die cast. *Arid Zone Journal of Engineering, Technology and Environment, 20*(4), 828–835.

Yang, F., Li, H., & Jiang, Y. (2025). A review of pressure regulation technologies for irrigation pipeline systems. *Agriculture, 15*(14), 1528. https://doi.org/10.3390/agriculture15141528